Modeling on Fragmentation of Clusters inside a Mass Spectrometer

Zapadinsky, Evgeni

2019-01-17

Zapadinsky , E , Passananti , M , Myllys , N , Kurten , T & Vehkamäki , H 2019 , ' Modeling on Fragmentation of Clusters inside a Mass Spectrometer ' , Journal of Physical Chemistry A , vol. 123 , no. 2 , pp. 611-624 . https://doi.org/10.1021/acs.jpca.8b10744

http://hdl.handle.net/10138/298779
https://doi.org/10.1021/acs.jpca.8b10744

unspecified
publishedVersion

THE JOURNAL OF PHYSICAL CHEMISTRY A

Article

Cite This: J. Phys. Chem. A 2019, 123, 611−624

pubs.acs.org/JPCA

Modeling on Fragmentation of Clusters inside a Mass Spectrometer

Evgeni Zapadinsky,[†] Monica Passananti,*[,†] Nanna Myllys,[†,§] Theo Kurtén,[‡] and Hanna Vehkamäki[†]

[†]Institute for Atmospheric and Earth System Research/Physics, Faculty of Science, University of Helsinki, Helsinki, Finland

[‡]Institute for Atmospheric and Earth System Research/Chemistry, Faculty of Science, University of Helsinki, Helsinki, Finland

Supporting Information

ABSTRACT: Atmospheric clusters are weakly bound and can fragment inside the measuring instruments, in particular, mass spectrometers. Since the clusters accelerate under electric fields, the fragmentation cannot be described in terms of rate constants under equilibrium conditions. Using basic statistical principles, we have developed a model for fragmentation of clusters moving under an external force. The model describes an energy transfer to the cluster internal modes caused by collisions with residual carrier gas molecules. As soon as enough energy is accumulated in the cluster internal modes, it can fragment. The model can be used for interpreting experimental measurements by atmospheric pressure interface mass spectrometers.

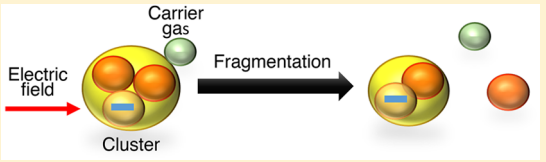

1. INTRODUCTION

The mass spectrometer and ion mobility spectrometer are effective tools for studying atmospheric clusters, e.g., measuring their composition and to some extent concentration.[1−3] These instruments are capable of resolving the elemental composition of sub-3-nm particles.[4,5] High-resolution and high-sensitivity mass spectrometers have increased our knowledge of individual charged clusters at ambient concentrations. However, some clusters might not be stable enough to survive severe conditions inside the instruments, and this might alter the detected distribution. Therefore, it is possible that measurements do not give a true picture of the clusters in both the atmospheric and laboratory experiments.

The trajectory of ions in mass spectrometers and ion mobility spectrometers is mostly defined by parameters like electric field, number concentration of the carrier gas, its temperature, flux, etc. The use of models such as ACDC (atmospheric cluster dynamic code)[6] to describe cluster transformations inside mass spectrometers is not possible. The ACDC model has been designed to describe the kinetics of formation and growth of atmospheric clusters. The model assumes the environment to be in equilibrium, but this is not the case in the mass spectrometer measurements. Although comparison with experiments has shown it to be quite successful,[1] there are still uncertainties in interpreting the atmospheric measurements and experimental results. Often, the discrepancies observed between the clusters distribution predicted by models such as ACDC and those measured by mass spectrometers have been attributed to possible cluster fragmentation inside the mass spectrometer.[7] The ionic clusters inside a mass spectrometer are accelerated under an electric field and experience collisions with carrier gas molecules. These collisions lead to energy redistribution between the colliding molecules and between the translational, rotational, and vibrational modes of the ionic clusters. As soon as the vibrational modes accumulate enough energy, the ionized clusters can get fragmented. This process resembles collision-induced dissociation (CID). CID is used in tandem mass spectrometry mainly to elucidate the structure of the analyzed ions.[8] An essential difference between a cluster and a molecule is in the strength of the bonds, so it is misleading to use the term dissociation for noncovalently bound molecular clusters when they fragment.

The cluster distribution measured by a mass spectrometer can be different from the one in the atmosphere due to collision induced cluster fragmentation (CICF) in the instrument. To investigate this possible artifact, we have developed a model for studying the influence of collisions between ionic clusters and carrier gas molecules on the clusters' fragmentation in atmospheric pressure interface time of flight (APiTOF) mass spectrometers. The ionic clusters are guided by electric fields inside the atmospheric pressure interface (APi) through a series of three vacuum chambers before arriving to the time of flight (TOF) mass spectrometer. A detailed description of the instrument is reported elsewhere.[5] Using a trimer cluster consisting of two sulfuric acid molecules and a bisulfate anion as an example, we model collision induced energy transfer between the translational, rotational and vibrational modes of the cluster, which can lead to cluster fragmentation.

Besides the introduction this article has four more sections: Theoretical Background of the Model, Details of Simulations, Results and Discussion, and Conclusion. Some material is placed in the Supporting Information. In particular, we have included a list of symbols in the Supporting Information.

Received: November 4, 2018
Revised: December 10, 2018
Published: December 14, 2018

DOI: 10.1021/acs.jpca.8b10744
J. Phys. Chem. A 2019, 123, 611−624

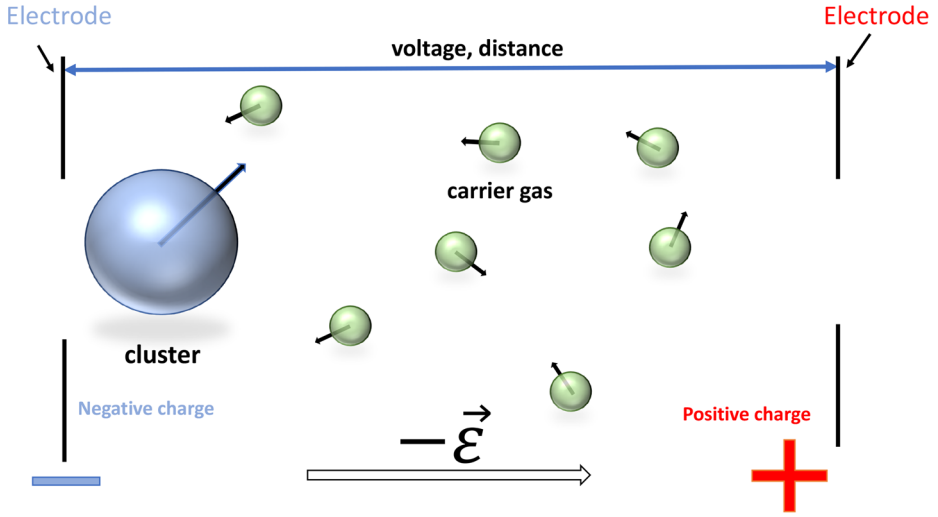

Figure 1. General setup of the model.

2. THEORETICAL BACKGROUND OF THE MODEL

2.1. General Description of the Model. The simplest setup for modeling CICF in some part of the mass spectrometer is as depicted in Figure 1. The negatively charged ionized cluster (later we usually refer to it as "cluster" omitting "ionic" or "ionized") moves under an applied constant and uniform electric field from one point to another. The electric field is along the z-axis, and the particular choice of direction of x- and y-axes is unimportant. The cluster also experiences collisions with the carrier gas molecules. Usually the carrier gas in APiTOF mass spectrometers is air. Typically, experiments are performed under stationary conditions when the flux, pressure, and temperature do not depend on time at any point in any of the chambers of the mass spectrometer. Thus, we have chosen to model the stationary conditions. We focus on the description of the collisions of the clusters with carrier gas molecules, energy transfer at collisions and energy redistribution during the time between the collisions which can lead to fragmentation. To avoid additional complications when developing the framework of the model, we keep the electric field constant in time and uniform in space and we also assume the velocity distribution of the carrier gas molecules to be Maxwellian. Alternating electric fields, magnetic fields, and deviations from the Maxwellian distribution can be straightforwardly included in the model.

We simulate the trajectory of the clusters moving from one electrode to another. The traveling trajectory is defined by the electric field and random collisions with the carrier gas molecules. Each cluster is considered individually. Its velocity, angular velocity, trajectory, and vibrational energy are monitored, and the probability of fragmentation is calculated along the trajectory. There are two possible fates for each cluster: (1) it can reach the second electrode or (2) it can get fragmented earlier. The aggregate data on the parameters along the trajectory as well as cluster's final fate are called a realization of the random process. After running a statistically significant set of realizations, we calculate the proportion of the fragmented clusters. Each realization includes several events and situations that can be viewed as random. They are related to collision, energy transfer at collisions and possible fragmentation. We consider these three processes and derive the related probability density functions (PDF) in the next three subsections.

2.2. Collision Probability Density Functions. In this subsection, we determine PDF, which provide the random values for the velocity vector of the carrier gas molecule colliding with the cluster, for the point of collision on the cluster surface, and for the time between the collisions. We treat both the cluster and the carrier gas molecule as spheres of radii R and R_g, respectively. When calculating the collision frequency, we consider the collision of the effective sphere with radius $\mathcal{R} = R + R_g$ and a point-like particle. The mass of the effective sphere M is equal to the mass of the cluster and the mass of the point-like particle m is equal to the mass of the carrier gas molecule. Substitution of the two colliding spheres problem with the problem of the collision of a sphere with the point-like particle does not change the value of the collision frequency.

The PDFs of the velocity component of the carrier gas molecule normal to the cluster surface u_n, of the polar angle between the cluster velocity vector and the vector drawn from the center of the cluster to the point of collision θ (see Figure 2), and of the time between collision t can be found by solving the collision frequency of the cluster moving with velocity v through a Maxwellian carrier gas. The solution can be found in the Supporting Information, here we present only the results. The PDF of the normal component of the carrier gas velocity u_n and of the angle θ at collision is

$$f_0(\theta, u_n) = \frac{1}{\Upsilon} 2\pi n \mathcal{R}^2 \sqrt{\frac{m}{2\pi kT}} (u_n + v\cos\theta) \exp\left(-\frac{m u_n^2}{2kT}\right) \sin\theta \quad (1)$$

where n is the number density of the carrier gas, k is the Boltzmann constant, T is the temperature, v is the cluster velocity, and Υ is the total collision frequency given by the following formula

$$\Upsilon = \pi \mathcal{R}^2 n \left(\left(\frac{kT}{mv} + v\right) \mathrm{erf}\left(\sqrt{\frac{m}{2kT}} v\right) + \sqrt{\frac{2kT}{\pi m}} \exp\left(-\frac{mv^2}{2kT}\right)\right) \quad (2)$$

DOI: 10.1021/acs.jpca.8b10744
J. Phys. Chem. A 2019, 123, 611−624

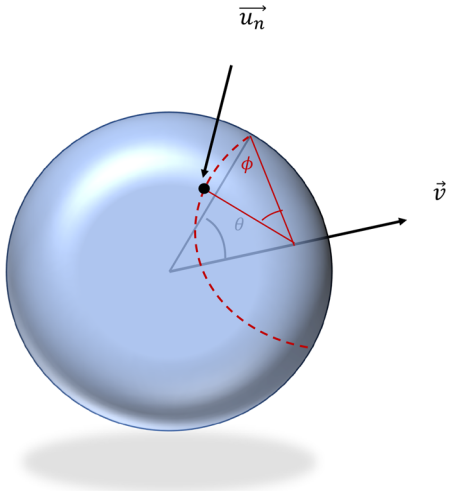

Figure 2. Illustration of the angles defining the point of collision between the carrier gas molecule and the cluster on its surface. The point of collision is marked with a black dot.

where erf is the error function. Naturally, Υ is approaching $\pi\mathcal{R}^2 n\sqrt{\frac{8kT}{\pi m}}$ at small v (to calculate the limit one needs to expand erf into a Taylor series). This corresponds to the collision frequency of Maxwellian gas with a motionless sphere. In the opposite limiting case, Υ is approaching $\pi\mathcal{R}^2 nv$ at very large v, which corresponds to collision of the sphere moving with velocity v through a motionless gas. The dependence of the collision frequency on the velocity of the cluster is presented in Figure 3. The PDF of the azimuth angle ϕ (see Figure 2) is even, and the PDF of the component of the carrier gas molecule velocity tangential to the cluster sphere obeys a two-dimensional Maxwell distribution.

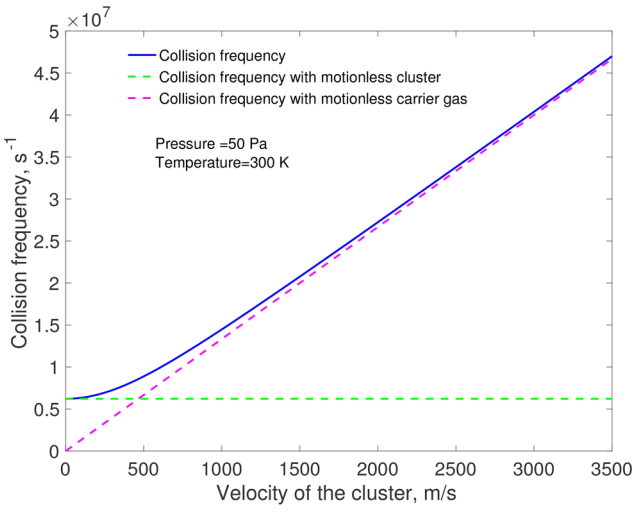

Figure 3. Dependence of the collision frequency of the cluster with the Maxwellian gas at 300 K on the velocity of the cluster.

The PDF of the time between collisions is

$$f_c(t) = \Upsilon(t)\exp\left(-\int_0^t \Upsilon(t)\,dt\right) \tag{3}$$

The total collision frequency $\Upsilon(t)$ depends on time because the velocity of the cluster moving in the electric field is not constant. Between the collisions the velocity is defined by

$$\vec{v} = \vec{v}_0 + \frac{q\vec{\mathcal{E}}}{M}t \tag{4}$$

where $\vec{v}_0$ is the velocity right after the previous collision, or at the beginning of the simulation, q is the charge of the cluster, and $\vec{\mathcal{E}}$ is the electric field.

2.3. Energy Transfer at Collisions. At first we consider the time scales of the processes related to collisions. The collision of clusters with carrier gas molecules is possible only in the first two chambers of the APiTOF mass spectrometer. The pressure there ranges from 1 to 200 Pa. The voltages between the consecutive electrodes there do no exceed 17 V. Thus, we can estimate the upper limit of the velocity v for a cluster with a mass of about 300 au to be about 3000 m/s. Therefore, considering that the typical time between the collisions of the cluster with the carrier gas molecules equals $1/\Upsilon$, we estimate it to be in the range between 10^{-5} and 10^{-8} s (see eq 2 and Figure 3). When collision happens, the cluster and the carrier gas molecule form a "collisional complex". Since the interaction between the colliding parties is weak, the lifetime of the "collisional complex" can be determined either by the time for the carrier gas molecule needed to pass 1−2 Å or by the lowest vibrational frequencies of the cluster. In both cases, we obtain the lifetime of the "collisional complex" to be on the order of 10^{-12} s.

The energy transfer at collision of two molecules as well as energy redistribution after collisions have been intensively studied for many years. Quantum effects are essential in the collision of molecules. The vibrational frequencies are relatively high, and the gaps between the energy levels are usually much higher than kT. In case of clusters, the situation is different. Some frequencies are low, and even at room temperatures quite many vibrational modes are unfrozen. As one can see from the Supporting Information, already 12 vibrational modes of the trimer under study are unfrozen at room temperatures. Thus, the energy spectrum even at room temperature is continuous, and energy transfer between the modes is not hindered. For any amount of transferring energy, there are always available energy states. We assume that the microcanonical principle holds, so that all states having the same energy can be observed with an equal probability. Therefore, the amount of energy transferred to the vibrational modes of the cluster is defined by the densities of states and the conservation of momentum, angular momentum and energy. The rotational and vibrational degrees of freedom of the carrier gas molecules are neglected.

Similarly to molecular rotational frequencies, the rotational frequencies of the cluster are much lower than the vibrational ones. Therefore, postcollisional energy transfer in the cluster is much faster for vibrational−vibrational energy exchange than for rotational−vibrational energy exchange. This has been confirmed by a molecular dynamics study[9] of argon clusters. Translational−vibrational and vibrational−vibrational energy transfer occurs at the time scales comparable to reverse vibrational frequencies, while rotational−vibrational energy transfer takes 10−100 times longer. It was noted in the same study that the tangential component of the colliding molecule's velocity mostly enhances rotation rather than vibration. Therefore, when writing equations for the normal components,

DOI: 10.1021/acs.jpca.8b10744
J. Phys. Chem. A 2019, 123, 611−624

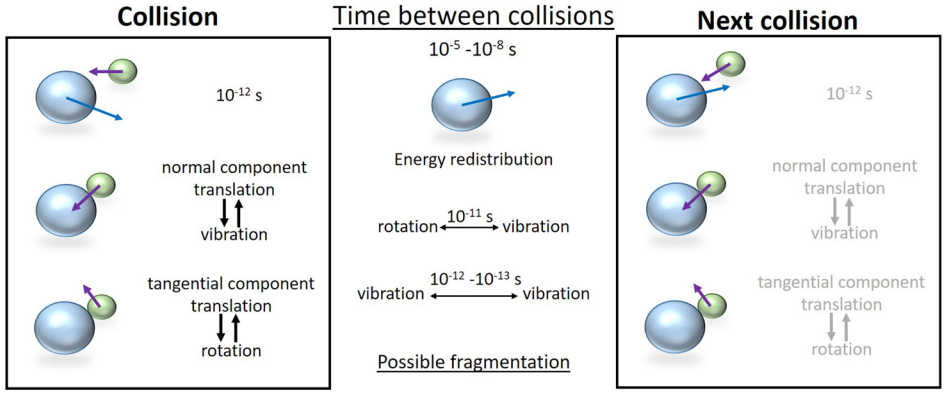

Figure 4. Time scales of the processes related to collision of the cluster (blue sphere) with the carrier gas molecule (green sphere), energy transfer process induced by the normal and tangential components of the carrier gas molecule velocity, and energy redistribution.

we do not consider rotational−vibrational energy transfer. Similarly, for the tangential components, we do not consider energy transfer from the translational mode of the carrier gas molecule to the vibrational motion of the cluster. After collision, we consider energy redistribution between vibrational and rotational degrees of freedom of the cluster, as this happens on a much faster time scale than the time between collisions of the cluster and carrier gas molecules. The time scales of the energy transfer and redistribution are summarized in Figure 4.

The different time scales of the processes allow us to build a simple model for describing energy transfer at collisions. In this model, they can be characterized as "instant inelastic collisions". It is convenient to consider the collision in the system of coordinates where the cluster center of mass is at rest just before the collision. Since the rotational−vibrational energy interchange can be neglected during the lifetime of the "collisional complex", we can split our system, consisting of the motional modes of the cluster and the carrier gas molecule, into two closed subsystems for which conservation of energy can be considered separately. The first subsystem includes the component of the carrier gas molecule translational motion normal to the cluster surface, and the vibrational modes of the cluster. The second subsystem includes the component of the carrier gas translational motion tangential to the cluster surface and the rotational modes of the cluster.

The collision time (lifetime of the "collisional complex") is very short, so the position of the carrier gas molecule and the cluster do not noticeably change while they stay together in the "collisional complex". We assume the same for orientation of the "collisional complex" and this is in line with the time scales of the processes shown in Figure 4. When the "collisional complex" decays, we assume that in the first subsystem the direction of the velocities of the cluster and the carrier gas are collinear with the velocity component of the carrier gas molecule normal to the cluster surface just before the collision. The additional physical assumption made here is that the cluster vibrational modes return the energy to the translational motion of the carrier gas molecule along the same line as they receive it. Note that this assumption affects only the direction of the motion after collisions, not the amount of energy transferred to the cluster.

First, we consider the conservation laws for the first subsystem. According to the conservation of momentum and energy, the carrier gas molecule sticks to the cluster, so that the "complex" acquires the velocity $v'_{com} = \frac{m}{M+m}u'_n$ and energy $\mu u_n'^2/2$, where $\mu = \frac{mM}{m+M}$ is the reduced mass, and prime in the notations of the velocities means that they are measured in the system of coordinates moving with the same velocity as the center of mass of the cluster just before the collision. Since we do not consider rotational−vibrational energy transfer during the lifetime of the "collisional complex", we can omit rotational energy, and write the energy of the complex $E_{com} = \epsilon_{v0} + \mu u_n'^2/2$, where ϵ_{v0} is the vibrational energy of the cluster just before the collision. After the cluster and the carrier gas molecule separate, part of the energy E_{com} goes to the translational energy of the relative motion of the separating parties, while the rest stays in the vibrational modes of the cluster. According to microcanonical principle this division is defined by the density of states. The combined density of states of vibrational and relative translational motion can be written as

$$\rho_{com}(E_{com}) = \int_0^{E_{com}} \rho_t(\epsilon_t)\rho_v(E_{com} - \epsilon_t)\, d\epsilon_t \tag{5}$$

where $\rho_t(\epsilon_t)$ is the density of states of the relative translational motion of the cluster and the carrier gas molecule, $\rho_v(\epsilon_v)$ is the vibrational density of states of the cluster, $E_{com} = \epsilon_v + \epsilon_t$, ϵ_v is the vibrational energy of the cluster right after collision, and ϵ_t is the energy of the relative translational motion of the cluster and the carrier gas molecule. The energy is counted from the zero-point energy of the cluster. The integrand, when normalized, is the PDF to observe a certain energy in the relative translational motion of the cluster and carrier gas molecule after collision $f_n(\epsilon_t)$ (for a more detailed derivation of this PDF see the Supporting Information). The normalization constant is $\rho_{com}(E_{com})$. The density of states of the relative translational motion can be written as[10]

$$\rho_t(\epsilon_t) = \frac{4\sqrt{2}\pi V\mu^{3/2}\sqrt{\epsilon_t}}{(2\pi\hbar)^3} \tag{6}$$

where V is the volume of the system and $\hbar$ is the reduced Planck constant. The cluster vibrational density of states can be calculated numerically (for description of the method see section 3). Hence,

$$f_n(\epsilon_t) = \frac{\rho_v(E_{com} - \epsilon_t)\sqrt{\epsilon_t}}{\int_0^E \rho_v(E_{com} - \epsilon_t)\sqrt{\epsilon_t}\, d\epsilon_t} \tag{7}$$

When making simulations we draw a random value of ϵ_t from the distribution given by eq 7. Because of conservation of

DOI: 10.1021/acs.jpca.8b10744
J. Phys. Chem. A 2019, 123, 611−624

energy the vibrational energy of the cluster right after collision is

$$\epsilon_v = \epsilon_{v0} + \mu u_n'^2/2 - \epsilon_t \tag{8}$$

The convenient system of coordinates for considering conservation laws for the second subsystem is formed by the mutually orthogonal unit vectors $\vec{i}, \vec{j}$ and $\vec{k}$ depicted in Figure 5.

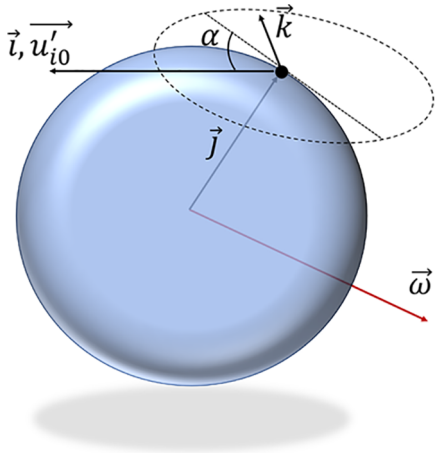

Figure 5. Directions of the axes *i*, *j*, *k*. The dashed tangential line drawn through the point of collision (black dot) is in the plane formed by vector of the cluster velocity and by the vector drawn from the center of the sphere to the point of collision. The direction of the axis *i* is collinear with the vector of the tangential velocity of the carrier gas molecule u'_{i0}.

Note that the *j*-component of the angular velocity of the cluster ($\vec{\omega}$) stays unchanged during the collision, and does not affect the velocities of either the cluster or the carrier gas molecule. The other components are involved in two independent sets of equations

$$\begin{gathered} Rmu'_{i0} + I\omega_{k0} = I\omega_k + Rmu'_i \\ mu'_{i0} = Mv'_i + mu'_i \\ \frac{mu_{i0}'^2}{2} + \frac{I\omega_{k0}^2}{2} = \frac{mu_i'^2}{2} + \frac{I\omega_k^2}{2} + \frac{Mv_i'^2}{2} \end{gathered} \tag{9}$$

and

$$\begin{gathered} I\omega_{i0} = I\omega_i + Rmu'_k \\ 0 = Mv'_k + mu'_k \\ \frac{I\omega_{i0}^2}{2} = \frac{mu_k'^2}{2} + \frac{I\omega_i^2}{2} + \frac{Mv_k'^2}{2} \end{gathered} \tag{10}$$

where the index 0 indicates that the value is taken just before the collision and

$$I = \frac{2}{5}MR^2 \tag{11}$$

is the moment of inertia of the cluster (solid sphere). The sets of eqs 10 and 11 imply that collisions occur under conditions when there is no sliding of the carrier gas molecule over the cluster. This maximizes the energy transfer between the translational and rotational modes of motion. The solution of these sets of equation gives the components of the velocity and angular velocity for the cluster right after collision with the carrier gas molecule:

$$\begin{gathered} v'_i = \frac{4m(u'_{i0} - \omega_{k0}R)}{2M + 7m} \\ \omega_k = \omega_{k0} + \frac{10m(u'_{i0} - \omega_{k0}R)}{R(2M + 7m)} \end{gathered} \tag{12}$$

and

$$\begin{gathered} v'_k = -\frac{4m\omega_{i0}R}{2M + 7m} \\ \omega_i = \frac{(2M - 3m)\omega_{i0}}{2M + 7m} \end{gathered} \tag{13}$$

Naturally, the solution of the sets of eqs 10 and 11 gives also values of the velocities of the carrier gas molecules. Since we do not use them in this study, they are not presented. We neglect the effect of collisions with clusters on the velocity distribution of the carrier gas molecules. Eqs 12 and 13 allow one to calculate the change of rotational energy of the cluster at the collision. Suppose that just before the collision the rotational energy of the cluster has the value ϵ_{r0}. Then, the rotational energy of the cluster right after collision is

$$\epsilon_r = \epsilon_{r0} + \frac{I(\omega_i^2 - \omega_{i0}^2)}{2} + \frac{I(\omega_k^2 - \omega_{k0}^2)}{2} \tag{14}$$

Redistribution of energy between rotational and vibrational degrees of freedom can be described similarly to translational–vibrational energy exchange considered earlier. The rotational density of states is[10]

$$\rho_r(\epsilon_r) = \frac{4\sqrt{2}I^{3/2}}{\hbar^3}\sqrt{\epsilon_r} \tag{15}$$

Assuming the microcanonical principle to work for rotational–vibrational microstates of the cluster, we can write the PDF of the rotational energy of the cluster:

$$f_r(\epsilon_r) = \frac{\rho_v(E - \epsilon_r)\sqrt{\epsilon_r}}{\int_0^E \rho_v(E - \epsilon_r)\sqrt{\epsilon_r}\,d\epsilon_r} \tag{16}$$

where $E = \epsilon_r + \epsilon_v$ is the cluster internal energy. If fragmentation does not happen before the next collision, the rotational energy just before the next collision is determined by a random value obtained from the PDF of eq 16.

The ionized clusters in mass spectrometers accelerate under electric fields. The center of charge of the cluster does not necessarily coincide with its center of mass. This leads to pendulum type vibration around the center of charge. Indeed, if we use the coordinate system attached to the center of charge, the center of mass experiences an inertial force *Ma*, where *a* is acceleration of the cluster. Hence, we observe a physical pendulum vibration with frequency on the order $\sqrt{a/l}$, where *l* is the distance between centers of charge and mass. This frequency at accelerations typical for mass spectrometers is about 1 order of magnitude smaller than rotational frequencies of the clusters under study. In some conditions this type of motion can be important, and should not be forgotten, but in the present study these vibrations are neglected.

2.4. Cluster Fragmentation Rate. Because of the intracluster energy exchange between the modes, a large part

DOI: 10.1021/acs.jpca.8b10744
J. Phys. Chem. A 2019, 123, 611–624

of the internal energy can be localized in particular bonds. This can lead to the cluster fragmentation. RRKM[11−14] theory of unimolecular reactions provides a tool for calculation of the fragmentation rate.[15] The probability that enough energy to break the cluster or molecule is accumulated in the weakest bonds is one of the key values in this theory. In terms of the phase-space theory,[16] the cluster is considered to be broken when a specific area of the phase space is reached. In the present study, we use mostly the language of phase-space theory of chemical reactions, however, we sometimes invoke RRKM language for illustrative purposes. Accompanied with the detailed balance approached developed by Weisskopf[17] for description of neutron escape from a potential well, the phase space theory of chemical reactions allows one to calculate the cluster fragmentation rate.[18]

The detailed balance approach allows one to express the fragmentation rate through the reverse reaction of sticking of the fragmentation products. In our case, the cluster is the trimer AAB, where A stands for sulfuric acid H_2SO_4, and B denotes the bisulfate anion HSO_4^-. The prevailing fragmentation channel of this cluster is

$$\mathrm{AAB} \rightarrow \mathrm{AB} + \mathrm{A} \tag{R1}$$

The fragmentation energy for reaction R1 is 29.3 kcal/mol. Other fragmentation pathways, having fragmentation energies 58.1 and 76.4 kcal/mol, can hardly be observed in the mass spectrometer.[19] The energy required for detachment of the electron from B is 109.5 kcal/mol.[20] This makes the detachment of the electron from the cluster to be also improbable in the mass spectrometer.

As was mentioned in subsection 2.3, we count the internal energy of the cluster E from the zero-point energy of the cluster. However, the zero-point energy of the products is higher, and the difference between the zero-point energies is the fragmentation energy E_f. If $E < E_f$ fragmentation cannot happen. For the total energy of the products (including their relative translational, rotational and vibrational motions) it is convenient to introduce the energy ε counted from the zero-point energy of the products. Since energy is conserved in the process of fragmentation $E_f + \varepsilon = E$.

Suppose we have a microcanonical ensemble consisting of N_{tot} isolated clusters having the same internal energy E. Each cluster is placed in a box with volume V, clusters can be fragmented, and the products of the fragmentation can merge again to form the initial cluster. If we wait long enough, we observe a detailed balance between the initial clusters and products, which can be written as

$$\gamma(\varepsilon)N(E_f + \varepsilon) = k_p(\varepsilon)N_p(\varepsilon) \tag{17}$$

where $\gamma(\varepsilon)$ is the fragmentation rate constant, $k_p(\varepsilon)$ is the rate of the reverse process of cluster formation from the fragmentation products, $N(E_f + \varepsilon)$ is the number of boxes where the cluster is intact, and $N_p(\varepsilon)$ is the number of boxes where the cluster is fragmented. Eq 17 is a sum of similar equations for individual microstates for both the left and the right-hand side. Since the boxes are isolated energy, momentum and angular momentum are conserved. The reverse of reaction R1 (recombination of the fragmentation products) is thought to be barrierless,[21] and the reaction rate simply equals the collision rate. Therefore, taking into account that the time between collisions of clusters with carrier gas molecules ranges between 10^{-5} and 10^{-8} s (see subsection 2.3) it is natural to assume that the phase space of the system is properly explored. This allows us to assume that the ergodicity holds and all microstates having the same energy can be observed with equal probability, like in the microcanonical ensemble. Hence, we can write

$$\frac{N(E_f + \varepsilon)}{N_{tot}} = \frac{\rho(E_f + \varepsilon)}{\rho(E_f + \varepsilon) + \rho_{tot}(\varepsilon)} \tag{18}$$

and

$$\frac{N_p(\varepsilon)}{N_{tot}} = \frac{\rho_p(\varepsilon)}{\rho(E_f + \varepsilon) + \rho_{tot}(\varepsilon)} \tag{19}$$

where $\rho(E_f + \varepsilon)$ and $\rho_p(\varepsilon)$ are the densities of states, corresponding to the intact cluster and the fragmented cluster, respectively. Using eqs 18 and 19, we can rewrite eq 17

$$\gamma(\varepsilon)\rho(E_f + \varepsilon) = k_p(\varepsilon)\rho_p(\varepsilon) \tag{20}$$

Equation 20 allows us to calculate $\gamma(E)$, but first we have to calculate $\rho(E)$, $\rho_p(E)$, and $k_p(\varepsilon)$.

It is convenient to consider fragmentation in the system of coordinates, which moves with the same velocity as the center of mass of the cluster. Therefore, only rotational and vibrational densities of states are taken into account when calculating the total density of states of the cluster. Fragmentation occurs when too much energy is localized in a particular bond of the cluster, thus breaking it. The sources of this energy are other vibrational modes and rotational motion. As was mentioned in the previous subsection the energy exchange between rotational and vibrational modes is much slower than the energy exchange between different vibrational modes. In this case, the fragmentation rate constant can be written as a product of two factors: the first is the probability of a certain distribution of energy between the rotational and vibrational modes of the cluster $f_r(\epsilon_r)$ defined by eq 16, and the second is the fragmentation rate constant $\gamma_0(\varepsilon - \epsilon_r)$ at this certain energy distribution between the modes. All possible energy distributions must be summed up. We can thus write

$$\gamma(\varepsilon) = \int_0^{\varepsilon} f_r(\epsilon_r)\gamma_0(\varepsilon - \epsilon_r)\, \mathrm{d}\epsilon_r \tag{21}$$

Equation 21 defines a fragmentation rate constant which is independent of the rotational energy of the cluster. The rate constant $\gamma_0(\varepsilon - \epsilon_r)$ is independent of rotational energy, hence it describes the fragmentation of cluster which does not have angular momentum, indicated by index 0. The influence of the angular momentum on the fragmentation rate is taken into account through averaging of the rate constant $\gamma_0(\varepsilon - \epsilon_r)$ over the PDF to observe a certain rotational energy. For the rate $\gamma_0(\varepsilon - \epsilon_r)$ a similar equation to eq 20 can be written

$$\gamma_0(\varepsilon - \epsilon_r)\rho_v(E_f + \varepsilon - \epsilon_r) = k_p(\varepsilon - \epsilon_r)\rho_p(\varepsilon - \epsilon_r) \tag{22}$$

Now we have eliminated the translational and rotational motions from consideration, so the task to calculate the fragmentation rate constant has been reduced to the case when total momentum and angular momentum are zeros. Therefore, to complete the calculation of the fragmentation rate constant we need to find the formation rate constant when the total momentum and angular momentum of the products are zeros, and the total energy of the products equals to $\varepsilon - \epsilon_r$. We have previously assumed that the energy exchange between rotational and vibrational modes is much slower than the energy exchange between different vibrational modes, and that

DOI: 10.1021/acs.jpca.8b10744
J. Phys. Chem. A 2019, 123, 611−624

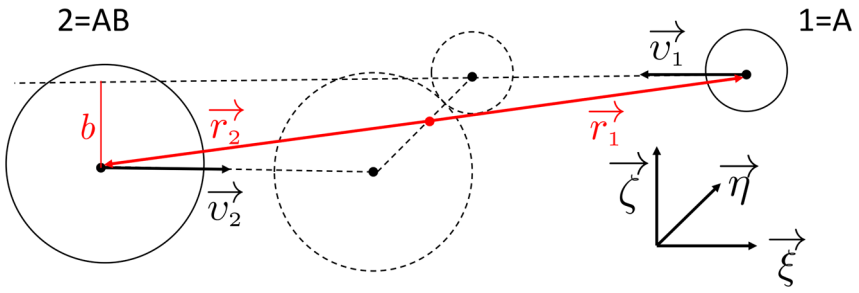

Figure 6. Schematic depiction of the product collision. The radius vectors of the colliding parties are drawn from the center of mass, which is marked with a red dot.

the recombination of the fragmentation products is barrierless. This considerably simplifies accounting for the angular momentum conservation. In more a general case, when the recombination reaction goes through a transition state and has a barrier, it requires much more efforts.[22−27]

When a cluster having no rotational and translational modes breaks into two fragments, six of its vibrational degrees of freedom transfer to rotational and translational degrees of freedom of the products. We illustrate this using the fragmentation reaction studied in this work. The cluster AAB has 54 vibrational degrees of freedom, the fragmentation product AB has 33 vibrational degrees of freedom and the product A has 15. The products altogether thus have 48 vibrational degrees of freedom, and the remaining six degrees of freedom have been transformed into rotational and translational degrees of freedom. Because of conservation of momentum and angular momentum, 12 translational and rotational degrees of freedom of the two products turn into six, since the total momentum and angular momentum are both zero.

We start by writing expressions for the rotational and translational energy of the products. For simplicity, we consider both fragmentation products as spheres, so that any directions can be selected to designate the principal moments of inertia, and we then use the observer's coordinates to write the expression for the rotational energy. The collision between the products is schematically depicted in Figure 6. Index 1 is related to A and index 2 to AB. We select the direction of the $\vec{\xi}$ axis as opposite to the direction of the relative velocity of the products $\vec{v} = \vec{v}_1 - \vec{v}_2$. The other two axes $\vec{\eta}$ and $\vec{\zeta}$ are perpendicular to each other and to $\vec{\xi}$, and collision occurs in the plane $\xi\zeta$. With such an arrangement, using the law of conservation of momentum and eq 24, we can write the conservation laws of angular momentum and energy in the form

$$\begin{aligned} L_{1\xi} + L_{2\xi} &= 0 \\ L_{1\eta} + L_{2\eta} + \sqrt{2\mu_p \varepsilon_t}\, b &= 0 \\ L_{1\zeta} + L_{2\zeta} &= 0 \\ \varepsilon_t + \varepsilon_r + \varepsilon_v &= E - \epsilon_r \end{aligned} \tag{23}$$

where L_ξ, L_η, L_ζ are the components of the angular momentum along the corresponding axes, labeled with indexes 1 and 2 for the fragmentation products A and AB, respectively. Their relative velocity v is expressed through the translational energy of the relative motion of the fragmentation products ε_t and their reduced mass μ_p as

$$v = \sqrt{\frac{2\varepsilon_t}{\mu_p}} \tag{24}$$

ε_v is the sum of vibrational energies of the products, b is the impact parameter as depicted in Figure 6, and the combined rotational energy of the products is

$$\varepsilon_r = \frac{{L_{1\xi}}^2}{2I_1} + \frac{{L_{1\eta}}^2}{2I_1} + \frac{{L_{1\zeta}}^2}{2I_1} + \frac{{L_{2\xi}}^2}{2I_2} + \frac{{L_{2\eta}}^2}{2I_2} + \frac{{L_{2\zeta}}^2}{2I_2} \tag{25}$$

where I_1, I_2 are the moments of inertia of the fragmentation products. After some algebra with the set of eq 23 and eq 25, we can write the combined rotational energy of the products as

$$\varepsilon_r = \frac{{L_{1\xi}}^2}{2I_p} + \frac{\left(L_{1\eta} + \frac{I_1 b\sqrt{2\mu_p \varepsilon_t}}{I_1 + I_2}\right)^2}{2I_p} + \frac{{L_{1\zeta}}^2}{2I_p} + \frac{\mu_p b^2}{I_1 + I_2}\varepsilon_t \tag{26}$$

where we have introduced a notation

$$\frac{1}{I_p} = \frac{1}{I_1} + \frac{1}{I_2} \tag{27}$$

The translational and rotational energies of the products are now expressed through three components of the angular momentum of one of the products and the energy of the relative translational motion of the products, which also has three components.

According to kinetic gas theory, the collision rate of the fragmentation products can be written as

$$\mathrm{d}k_p\,(\varepsilon - \epsilon_r) = \mathrm{d}\tau\ \mathrm{d}\mathcal{P}_{tr}\,(\varepsilon_t, \varepsilon_r|\varepsilon - \epsilon_r) \tag{28}$$

The probability of collision per unit time is

$$\mathrm{d}\tau = \frac{v}{V}\,\mathrm{d}\sigma \tag{29}$$

where the collision cross section $\mathrm{d}\sigma$ can be expressed through the impact parameter b (see Figure 6)

$$\mathrm{d}\sigma = 2\pi b\ \mathrm{d}b \tag{30}$$

The probability $\mathrm{d}\mathcal{P}_{\mathrm{tr}}(\varepsilon_t, \varepsilon_r|\varepsilon - \epsilon_r)$ to observe a certain energy distribution between the degrees of freedom of the fragmentation products, provided that their total energy is equal to $\varepsilon - \epsilon_r$, can be calculated as

DOI: 10.1021/acs.jpca.8b10744
J. Phys. Chem. A 2019, 123, 611−624

$$d\mathcal{P}_{tr}(\varepsilon_t, \varepsilon_r|\varepsilon - \epsilon_r) = \rho_{pt}(\varepsilon_t)\rho_{pr}(\varepsilon_r)\rho_{pv}(\varepsilon - \epsilon_r - \varepsilon_r - \varepsilon_t) \frac{d\varepsilon_t\, d\varepsilon_r}{\rho_p(\varepsilon - \epsilon_r)} \quad (31)$$

where $\rho_{pt}(\varepsilon_t)$, $\rho_{pr}(\varepsilon_r)$, and $\rho_{pv}(\varepsilon - \epsilon_r - \varepsilon_r - \varepsilon_t)$ are the densities of states of the relative and combined rotational and vibrational motions of the products, respectively. Using eqs 24 and 28 −31 we can write the cluster formation rate as

$$k_p(\varepsilon - \epsilon_r) = \frac{2\sqrt{2}\pi}{\rho_p(\varepsilon - \epsilon_r)\sqrt{\mu_p}V} \iiint_{\substack{0\le\varepsilon_r+\varepsilon_t\le\varepsilon-\epsilon_r \\ 0\le b\le b_{max}}} \sqrt{\varepsilon_t}\, b\, \rho_{pt}(\varepsilon_t)\rho_{pr}(\varepsilon_r)\rho_{pv}(\varepsilon - \epsilon_r - \varepsilon_r - \varepsilon_t)\, d\varepsilon_t\, d\varepsilon_r\, db \quad (32)$$

Integration over b in eq 32 is limited by the maximal impact parameter b_{max} leading to the formation of the cluster. Since AB is an ion and A has a dipole moment μ_D and polarizability α_A, the maximal impact parameter can be considerably higher than the sum of the radii of the colliding parties. Because of the attractive interaction the value of b_{max} depends on the translational and rotational energies of the fragmentation products.

The next step is to explicitly write the translational and vibrational densities of states. We can use an analogue of eq 6 for the density of states of the relative translational motion of the products

$$\rho_{pt}(\varepsilon_t) = \frac{4\sqrt{2}\pi V{\mu_p}^{3/2}\sqrt{\varepsilon_t}}{(2\pi\hbar)^3} \quad (33)$$

Since rotations of the two bodies are coupled due to angular momentum conservation it is sufficient to find the density of states of only one product. In this case, it is advantageous to express the rotational density of states through the components of the angular momentum rather than through the rotational energy, as was done in eq 15, resulting in[28]

$$\rho_{pr}(\varepsilon_r)\, d\varepsilon_r = \frac{dL_{1\xi}\, dL_{1\eta}\, dL_{1\zeta}}{\pi\hbar^3} \quad (34)$$

Using eqs 22, 32, 33, and 34, we obtain the fragmentation rate of a nonrotating cluster

$$\gamma_0(\varepsilon - \epsilon_r) = \frac{2\mu_p}{\pi^2\hbar^6\rho_v(E_f + \varepsilon - \epsilon_r)} \times \int\cdots\int_{\substack{0\le\varepsilon_{rt}\le\varepsilon-\epsilon_r \\ 0\le b\le b_{max}}} \varepsilon_t\, b\, \rho_{pv}(\varepsilon - \epsilon_r - \varepsilon_{rt})\, d\varepsilon_t\, dL_{1\xi}\, dL_{1\eta}\, dL_{1\zeta}\, db \quad (35)$$

where

$$\varepsilon_{rt} = \frac{{L_{1\xi}}^2}{2I_p} + \frac{\left(L_{1\eta} + \frac{I_1 b\sqrt{2\mu_p\varepsilon_t}}{I_1+I_2}\right)^2}{2I_p} + \frac{{L_{1\zeta}}^2}{2I_p} + \left(1 + \frac{\mu_p b^2}{I_1+I_2}\right)\varepsilon_t \quad (36)$$

is the sum of translational and rotational energies of the products (see eq 26). It is convenient to carry out a transformation of coordinates: $\varepsilon_t \to \widetilde{\varepsilon_t} = \left(1 + \frac{\mu_p b^2}{I_1+I_2}\right)\varepsilon_t$, $L_{1\xi} \to \widetilde{L_{1\xi}} = L_{1\xi}$, $L_{1\eta} \to \widetilde{L_{1\eta}} = L_{1\eta} + \frac{I_1 b\sqrt{2\mu_p\varepsilon_t}}{I_1+I_2}$ and $L_{1\zeta} \to \widetilde{L_{1\zeta}} = L_{1\zeta}$. The set of three variables $\{\widetilde{L_{1\xi}}, \widetilde{L_{1\eta}}, \widetilde{L_{1\zeta}}\}$ constitutes the Cartesian coordinates, and we can make a transformation to the spherical coordinate system. In spherical coordinates, integration over the angles can be performed. After changing variables and denoting

$$\widetilde{\varepsilon_r} = \frac{\widetilde{L_{1\xi}}^2}{2I_p} + \frac{\widetilde{L_{1\eta}}^2}{2I_p} + \frac{\widetilde{L_{1\zeta}}^2}{2I_p} \quad (37)$$

eq 35 reduces to

$$\gamma_0(\varepsilon - \epsilon_r) = \frac{8\sqrt{2}\mu_p {I_p}^{3/2}}{\pi\hbar^6\rho_v(E_f + \varepsilon - \epsilon_r)} \times \iint_{\substack{0\le\widetilde{\varepsilon_t}+\widetilde{\varepsilon_r}\le\varepsilon-\epsilon_r \\ 0\le b\le b_{max}}} \left(\frac{I_1+I_2}{I_1+I_2+\mu_p b^2}\right)^2 b\widetilde{\varepsilon_t}\sqrt{\widetilde{\varepsilon_r}}\rho_{pv}(\varepsilon - \epsilon_r - \widetilde{\varepsilon_t} - \widetilde{\varepsilon_r})\, d\widetilde{\varepsilon_t}\, d\widetilde{\varepsilon_r}\, db \quad (38)$$

As mentioned, the value of b_{max} depends on translational and rotational energies of the products due to interaction of the colliding parties. The lower the energies, the higher is b_{max}. Only this coupling prevents the analytical integration of eq 38 over b. We investigated how strongly the rate constant the rate constants depend on b_{max}. First, we set $b_{max} = \infty$ in all cases. Then eq 38 transforms to

$$\gamma_0(\varepsilon - \epsilon_r) = \frac{4\sqrt{2}{I_p}^{3/2}(I_1+I_2)}{\pi\hbar^6\rho_v(E_f + \varepsilon - \epsilon_r)} \times \iint_{0\le\widetilde{\varepsilon_t}+\widetilde{\varepsilon_r}\le\varepsilon-\epsilon_r} \widetilde{\varepsilon_t}\sqrt{\widetilde{\varepsilon_r}}\rho_{pv}(\varepsilon - \epsilon_r - \widetilde{\varepsilon_t} - \widetilde{\varepsilon_r})\, d\widetilde{\varepsilon_t}\, d\widetilde{\varepsilon_r} \quad (39)$$

We have compared eqs 38 and 39 using a relation, presented in the literature, between the microcanonical collision rate and the energies of colliding parties experiencing ion-dipole interaction. The microcanonical collision rate calculated by variational rate theory has been compared to numerical classical trajectory calculations.[29] The results of the theory are only about 10% higher than the numerical results. As we shall see later, even much larger variations in the fragmentation rate constant do not affect the main conclusions. Adapting the expression for the microcanonical capture rate constant calculated with variational rate theory to our notations, we can write

$${b_{max}}^2 = \sqrt{\frac{\mu_p}{2\varepsilon_t}}\, k_L g(w) \quad (40)$$

where $k_L = 2\pi q\sqrt{\alpha_A\mu_p}$ is the Langevin rate constant, and

DOI: 10.1021/acs.jpca.8b10744
J. Phys. Chem. A 2019, 123, 611−624

$$g(w) = \begin{cases} \frac{27}{1024w^{3/2}}(8w^2 - 20w - 1 + (8w+1)^{3/2}), & 0 \le w \le \frac{5}{9} \\ \frac{1}{9w^2}(2(9w^2 + 3w + 1)^{3/2} + (3w+2)(6w+1)(3w-1))^{1/2}, & \frac{5}{9} \le w \le \infty \end{cases} \quad (41)$$

where

$$w = \frac{2\alpha_A(\varepsilon_t + \varepsilon_{r1})}{\mu_D} \quad (42)$$

and ε_{r1} is the rotational energy of A. Note that the rotational energy of AB is not included in eq 42, as the charge is considered to be at the center of mass, and thus the rotation of AB does not affect the interaction of the products. Eqs 40, 41 and 42 allow us to perform a numerical integration of eq 38, taking into account the dependence of b_{max} on translational and rotational energies of the products due to the interaction between them. The comparison of eqs 38 and 39 in Figure 7 shows that the difference is negligible. Therefore, we have used eqs 39 in numerical calculations since it takes much less computing time than is required for integrating eq 38.

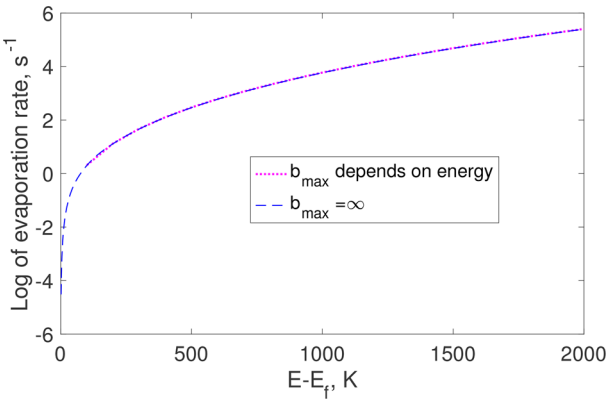

Figure 7. Dependence of the fragmentation rate constant of the cluster with zero angular momentum calculated on internal energy. It is calculated for two cases: (1) where maximal impact parameter is infinite and (2) where the value depends on the rotational and translational energies of the products.

The rate constant eq 21 calculated with eqs 16 and 39 allows us to obtain the probability for the cluster to stay intact until a certain time t

$$\mathcal{P}_{in}(t) = \exp(-\gamma(\varepsilon)t) \quad (43)$$

Hence the cumulative probability to get fragmented by time t is $F_f(t) = 1 - \mathcal{P}_{in}(t)$. Thus, the PDF of the fragmentation time can be written as

$$f_f(t) = \frac{dF_f(t)}{dt} = \gamma(\varepsilon)\exp(-\gamma(\varepsilon)t) \quad (44)$$

3. DETAILS OF THE MODEL AND SIMULATIONS

3.1. The Cluster and the Products Parameters and the Vibrational Densities of States. We have sampled the AAB potential energy surface by first creating 2800 input structures by randomly distributing molecules in space.[30] The structures were subsequently optimized using the semi-empirical PM6 method.[31] All converged structures were then reoptimized at the PW91/6-31+G* level of theory.[32] Different conformers were characterized based on electronic energies and dipole moments. 120 different structures were reoptimized and their frequencies were calculated using the PW91/6- 311+ +G** level of theory, and for the resulting conformers we computed zero-point-energy-corrected (ZPE-corrected) electronic energies.[33]

Since different levels of theory might yield different global minima, we selected 22 ZPE-corrected local minimum energy conformers. These structures were optimized and thermochemical parameters were calculated using the PW91 functional with a large aug-cc-pVQZ basis set. The lowest energy conformer for AAB was selected, and the normal mode vibrational frequencies as well as rotational constants for the principal axes were calculated approximating the cluster as a rigid rotor and harmonic oscillator. The electronic energy corrections were calculated on top of the DFT structure using the DLPNO−CCSD(T)/aug-cc-pVTZ level of theory with a tight pair natural orbital criteria.[34,35] The electronic energy corrections were computed using the Orca 4.0.1.2 program.[36] The fragmentation product AB was treated similarly. The vibrational frequencies and rotational constants are presented in the Supporting Information.

The vibrational densities of the states both for the cluster and the products have been calculated using the Beyer−Swinehart algorithm.[37] The algorithm is based on an exact recurrent relation, and the accuracy relies upon the width of energy bins for defining the density of states. They are recommended[38] to be smaller than 1 cm^{-1}. Thus, we use a value of 1 K (1 $cm^{-1} \simeq 1.44$ K). Additionally, we checked that densities of states calculated with Beyer−Swinehart algorithm match the ones calculated with direct counting method at low energies, and the densities of states calculated with an analytical formula[18] at high energies. The principal moments of inertia have obtained from rotational constants Θ_i using the relation

$$\Theta_i = \frac{\hbar^2}{2I_i k} \quad (45)$$

where $i = \beta, \delta, \lambda$ correspond to the principal rotational axes. When calculating the fragmentation rate constants and considering collisions, we approximate the cluster and the products of fragmentation as spheres. Therefore, it is reasonable to define the radius of the sphere using the relation (see eq 11)

$$\left(\frac{2}{5}MR^2\right)^3 = I_\beta I_\delta I_\lambda \quad (46)$$

where I_β, I_δ, and I_λ are the cluster principal moments of inertia. Eq 46 yields $R = 3.47$ Å for the AAB cluster.

The radii of the N_2 and O_2 molecules were calculated from the van der Waals volumes taken from a handbook.[39] For

DOI: 10.1021/acs.jpca.8b10744
J. Phys. Chem. A 2019, 123, 611−624

nitrogen, the radius is 2.49 Å and for oxygen it is 2.33 Å. Therefore, the average radius of the carrier gas molecule, according to the relative abundance of N_2 and O_2 in the atmosphere, is R_g = 2.46 Å. The air molecules interact with the cluster by ion-induced-dipole interactions. However, the effect of this long-range interaction on the collision frequency is negligible based on the values of the polarizability of N_2 and O_2.[40]

The fragmentation rate constant was calculated as described in subsection 2.4 by numerical integration for the values of energy separated by intervals of 1 K. The values of the rate constant inside these intervals has been obtained by linear interpolation. The temperature of the carrier gas was kept at 300 K. We average over 2000 realizations when calculating the fraction of fragmented clusters.

3.2. Simulation of Random Values. In our simulations, we frequently need to obtain the value of a random variable obeying some PDF. These functions are denoted by f with some index throughout this text (see eqs 3, 7, 16, and 44). We use a standard technique in all these cases. Suppose we have PDF $f(\chi)$ for the random variable χ defined in the interval from d to h. The cumulative probability $F(\chi)$ is defined by

$$F(\chi) = \int_d^{\chi} f(\chi')\, d\chi' \tag{47}$$

To obtain the value of the random variable χ we generate a random number c in the interval from 0 to 1, then solve the equation

$$F(\chi) = c \tag{48}$$

The solution of this equation χ_c is the value of the random variable obeying the PDF $f(\chi)$. In practice, to solve eq 48, we numerically integrate eq 47 until the integral reaches c, which gives us the value of the random variable. The method to obtain random values from two-dimensional PDF is based on probability theory,[41] and is described in the Supporting Information.

3.3. Scheme of Simulation.

1 We assign initial values for the coordinates, velocity, angular velocity and vibrational energy of the cluster. We have used random values from the Maxwell distribution at 300 K for the initial velocities of the cluster. Similarly, for initial angular velocity and vibrational energy of the cluster, we have used random values from the Boltzmann distribution at 300 K.

2 We calculate the time of the next collision using the PDF defined by eq 3. Before the collision, the cluster accelerates under an electric field.

3 We check whether the cluster is fragmented or not using the PDF defined by eq 44. If yes, we start from the item 1 for the new realization. If no, we calculate a new rotational energy using PDF 16 (changes due to rotational−vibrational energy exchange) and continue with item 4.

4 We define the point of collision on the surface of the cluster by the angle θ (Figure 2) using the PDF defined by eq 1 and the angle ϕ using an even PDF from 0 to 2π. Using the PDF defined by eq 1 and a two-dimensional Maxwellian PDF, we simulate normal and tangential components of the velocity of the colliding carrier gas molecule, respectively. Using an even PDF from 0 to 2π, we obtain the direction of the tangential component of the colliding carrier gas molecule (angle α in Figure 5). To consider the consequences of collision, we determine the direction of axes i, j, and k and define the projection of the cluster angular velocity onto these axes. We calculate new energies, velocity, and angular velocity of the cluster as described in subsection 2.3, and transfer the new velocity to laboratory coordinates.

5 We continue with items 2−4 until the cluster is fragmented or reaches the end point intact.

6 We start a new realization with item 1.

7 We calculate the fraction of the intact clusters after completing all realizations.

4. RESULTS AND DISCUSSION

In our model, the three essential factors determining the fragmentation of the ionized clusters are the number of collisions, the amount of energy transferred to the internal modes of the cluster at collisions and the fragmentation rate constant as a function of energy. First, we consider the fragmentation rate constant.

The dependence of the rate constant eq 21 on internal energy is presented in Figure 8. Figure 8 can be used to estimate the internal energy the cluster needs to be fragmented. As discussed in subsection 2.3, the time between the collisions of the cluster with carrier gas molecules at the conditions of an APiTOF mass spectrometer is in the interval 10^{-5}−10^{-8} s. Therefore, according to eq 43, we can expect a high probability for the cluster fragmentation when the rate constant is roughly in the interval 10^5−10^8 s. We can see from Figure 8 that such values are reached when the cluster's energy is from 2000 to 5500 K higher than the fragmentation energy (14744 K).

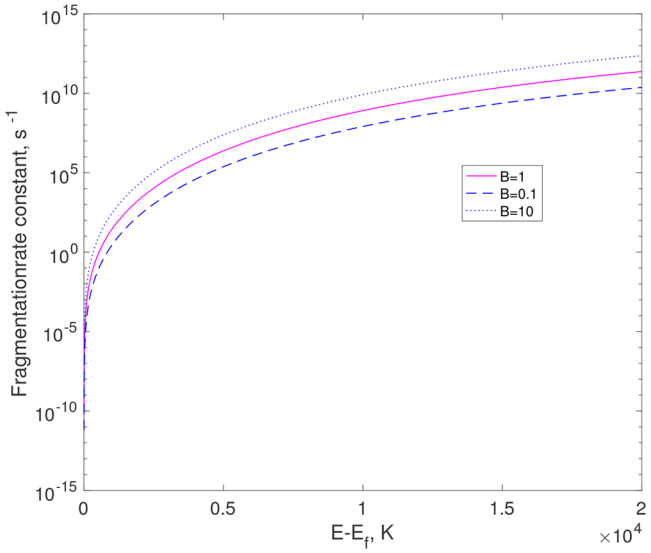

Figure 8. Dependence of the fragmentation rate on the internal energy. The meaning of parameter B is described in the text.

To study how the variation of the fragmentation rate constant affects the results of our model, we have multiplied it by an uncertainty factor B ranging from 10^{-3} to 10^3. The new rate constant $\gamma'(\varepsilon) = B\gamma(\varepsilon)$ has been fed to the model. The resulting fragmentation probabilities are presented in Figure 9. Changing the rate constant by 1 order of magnitude alters the degree of fragmentation by roughly 10%. Such a variation of

DOI: 10.1021/acs.jpca.8b10744
J. Phys. Chem. A 2019, 123, 611−624

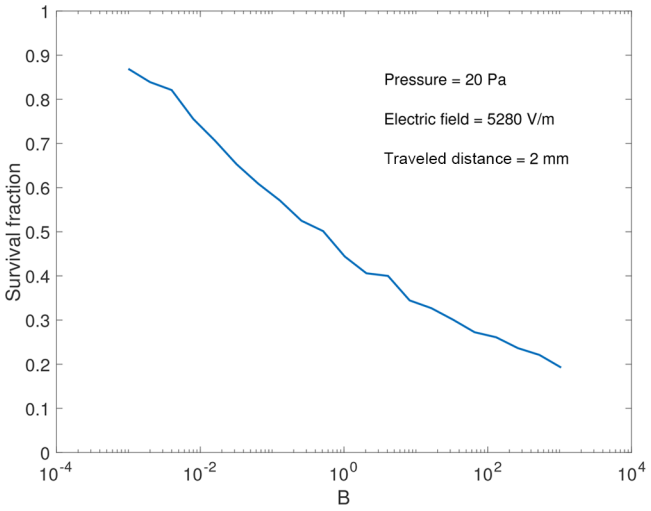

Figure 9. Effect of the uncertainty factor B of the fragmentation rate constant on the survival fraction.

the results is not significant, as it is close to the experimental error in studying the fragmentation inside mass spectrometers.[19] The weak effect of the rate constant variation can be explained by the relatively high amount of energy transferred in one collision. For example, under the conditions of Figure 10, the vibrational energy change per collision is about 1000 K just before fragmentation. Under the conditions of Figure 10b, the change is about 4000 K. This range of changes is typical for conditions of the APiTOF mass spectrometer. Because of such big leaps, the exact value of the limiting energy at which the cluster is fragmented is not significant. Figure 8 shows that the energies at which the rate constants $\gamma'(\varepsilon)$ and $\gamma(\varepsilon)$ have the same value in the interval $10^5 - 10^8$ s, differ roughly by 1000 K when $B = 10$ or $B = 0.1$. We can conclude that the results show moderate sensitivity to the values of the fragmentation rate constant.

The dependence of the degree of cluster fragmentation on pressure and the electric field are presented in Figure 11. The

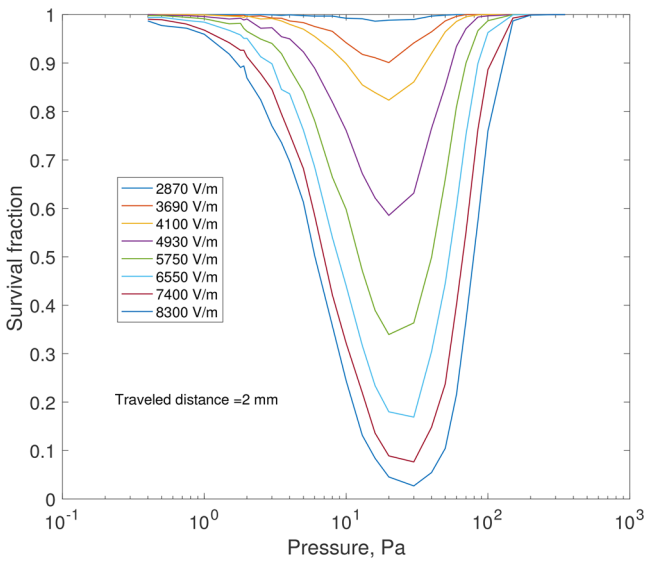

Figure 11. Dependence of the cluster fragmentation on pressure at different values of the electric field.

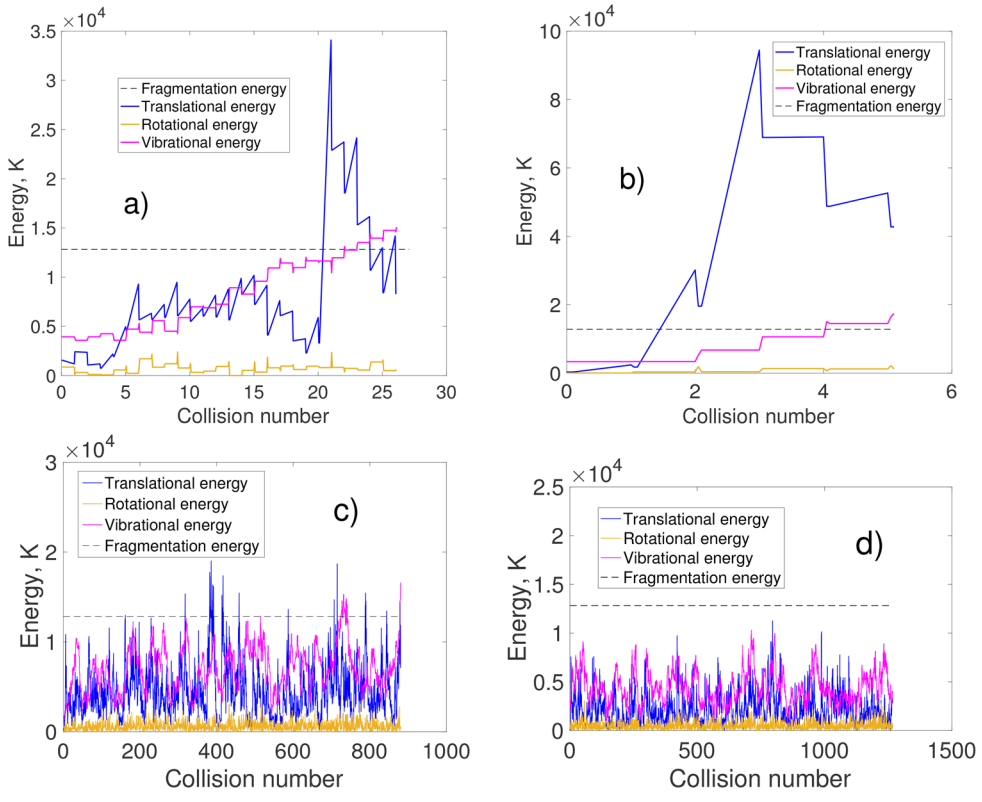

Figure 10. Cluster energy fluctuations during one realization at the carrier gas pressure and electric field: (a) 40 Pa and 4000 V/m, (b) 6 Pa and 5200 V/m, (c) 100 Pa and 5200 V/m, and (d) 100 Pa and 3200 V/m, respectively. In all cases, except part d, the cluster is fragmented.

DOI: 10.1021/acs.jpca.8b10744
J. Phys. Chem. A 2019, 123, 611−624

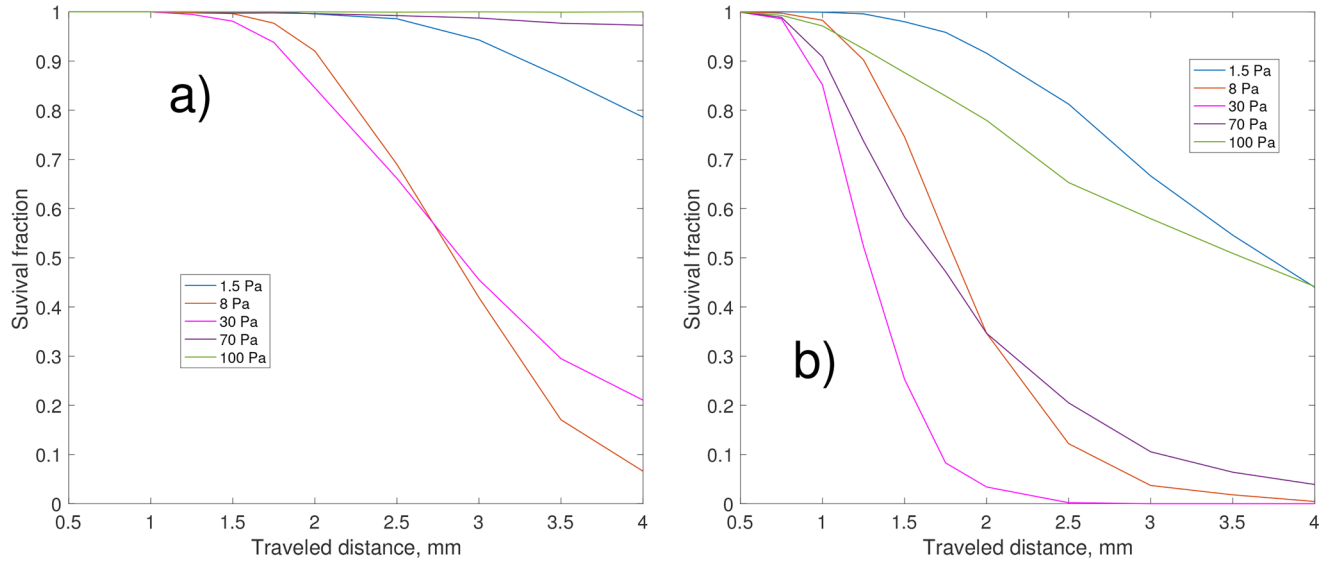

Figure 12. Dependence of the cluster fragmentation on the traveled distance at different pressures. The electric field is field is: (a) 4100 V/m, (b) 8300 V/m.

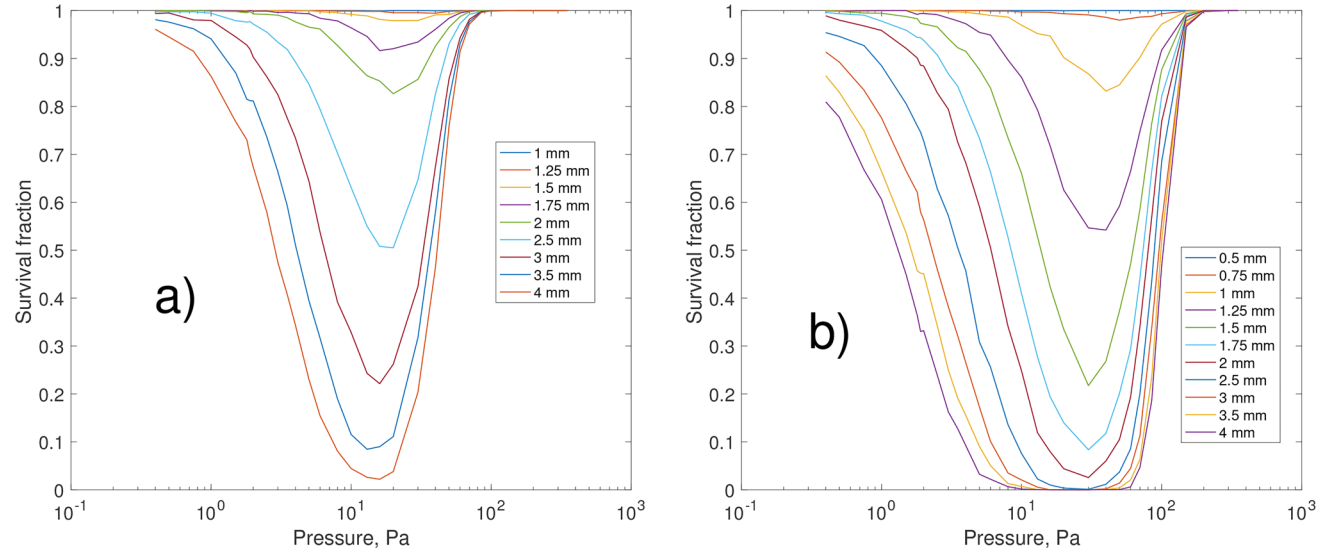

Figure 13. Dependence of the cluster fragmentation on pressure at different traveled distances. The electric field is: (a) 4100 V/m and (b) 8300 V/m.

figure shows that the clusters are fragmented at pressures ranging from 1 to 150 Pa with the traveled distance set to 2 mm. At higher than 150 Pa pressures, the clusters collide with carrier gas molecules frequently enough to establish a steady state drag velocity for the cluster. Hence, the translational energy of the cluster only fluctuates within certain limits, thus constraining also the internal energy to the certain limits. At lower pressures than 1 Pa, the clusters practically do not collide with carrier gas molecules while traveling the distance of 2 mm, so there is no chance for the translational energy to be transferred to internal energy, and fragmentation does not occur. The dependence of the fragmentation degree on the electric field is natural. The stronger the electric field, the more energy can be transferred to the internal modes of the cluster, increasing its chances to be fragmented.

As we can see from Figure 12, lengthening the traveled distance increases the degree of fragmentation. However, the rate of growth is different at low and high pressures. Comparing the curves of growth for two pressures having similar rates at short distances, we observe that the curve corresponding to lower pressure displays significantly higher fragmentation at long distances. There are two factors enhancing the fragmentation with lengthening traveled distances at low pressures. First, the longer the distance, the higher the probability to meet a collision partner. Second, the longer the distance, the higher the translational energy of the cluster at low pressures (see Figures 10a,b), because the steady state level for both translational and internal cluster energies is not reached before the cluster gets fragmented. Additionally, the higher the cluster translational energy, the more energy is transferred to its internal modes in one collision. We have observed that at pressures around or lower than 1 Pa, the amount of energy transferred in one collision to the internal modes reaches the level of 10000−15000 K when electric field is 5200 V/m. This is often enough for the cluster to fragment. At pressures 0.2−0.4 Pa, the amount of energy transferred in

DOI: 10.1021/acs.jpca.8b10744
J. Phys. Chem. A 2019, 123, 611−624

one collision reaches 30000−40000 K with the same electric field value.

At high pressures the picture is different. As we can see from Figure 13, the right borderline between the presence and absence of fragmentation shifts toward higher pressures much slower than the left borderline shifts toward the lower pressures when we increase the traveled distance. At high pressures, the cluster rather quickly reaches the steady state drag velocity. As we can see from Figure 10c, in this case the rotational and vibrational energy of the cluster do not grow either, they just fluctuate so that sometimes the internal energy is higher than the fragmentation energy and the cluster can be fragmented. Such situations correspond to the slow growth of fragmentation with increasing traveled distance. If the pressure is high enough (or the electric field is rather low), both the steady state level of the cluster internal energy and the amplitude of its fluctuation are such that fragmentation cannot happen. An example of this situation is presented in Figure 10d. Therefore, in this case the right borderline between fragmentation and nonfragmentation does not shift toward higher pressures with increasing traveled distance at all.

This observation has practical importance. Simulations are quite time-consuming at high pressures. To make a conclusion on the possible fragmentation there is no need to simulate the whole region between the electrodes, which can be several centimeters. It is enough to explore a small part of it, mapping whether or not the traveling cluster is in the steady-state regime, and whether or not its internal energy can reach the fragmentation level.

5. CONCLUSION

We have developed a model for studying the influence of collisions between ionic clusters and carrier gas molecules on the cluster fragmentation rate in atmospheric pressure interface time of flight (APiTOF) mass spectrometers. The model simulates the collision of a cluster with carrier gas molecules as it moves through the chambers of the mass spectrometer under an electric field. The translational energy can be transferred to the cluster internal modes in the collisions. If the cluster internal modes accumulate enough energy, the cluster can be fragmented. The collision, energy transfer, and fragmentation have been considered as random processes. Appropriate probability density functions have been calculated for all of them.

The probability density function for the collisions has been derived from kinetic gas theory. Energy transfer is governed by probability density function based on conservation laws and the microcanonical principle. The rotational and vibrational energy spectra of the cluster are practically continuous at the conditions of the mass spectrometer experiments. Therefore, energy transfer between the modes is not hindered, and it is defined by the densities of states. The latter have been calculated using the rigid-rotor-harmonic-oscillator approximation for the cluster minimum energy structures, which has been obtained from quantum chemistry calculations.

The probability of fragmentation is based on the fragmentation rate constant. The microcanonical fragmentation rate constant has been calculated on the basis of phase space theory for chemical reactions and the detailed balance principle. To take momentum and angular momentum conservation into account, we have assumed that rotational−vibrational energy exchange is much slower than vibrational−vibrational exchange. This has allowed us to reduce the problem to the calculation of the rate constant when the cluster angular momentum is zero. This considerably reduces the computational effort.

We have used the trimer consisting of two sulfuric acid molecules and one bisulfate anion as a model object for the fragmentation study inside the mass spectrometer. The dependence of the degree of cluster fragmentation on the distances between the electrodes, applied electric field and the residual carrier gas pressure has been examined. We have determined the pressure interval for typical APiTOF mass spectrometer electric fields and distances between the electrodes, at which the clusters may not survive. The clusters can be fragmented when the pressure is between 1 and 150 Pa. At higher than 150 Pa pressures, collisions are frequent enough to establish steady-state conditions for the internal cluster energy, which does not reach the level at which fragmentation is possible. At lower than 1 Pa pressures, collisions are too rare for fragmentation to occur in noticeable amounts.

The developed model has been successfully applied to the description of the experiments on the cluster fragmentation inside the APiTOF mass spectrometer. The results are to be published elsewhere.[19]

■ ASSOCIATED CONTENT

Supporting Information

The Supporting Information is available free of charge on the ACS Publications website at DOI: 10.1021/acs.jpca.8b10744.

Derivation of the probability density functions of variables related to collision frequency of the cluster with carrier gas molecules, derivation of the probability density function of the relative translational energy of the cluster and the carrier gas molecule right after collision, vibrational frequencies and rotational constants of the cluster and fragmentation products, and list of symbols (PDF)

■ AUTHOR INFORMATION

Corresponding Author

*(M.P.) E-mail: monica.passananti@helsinki.fi. Telephone: +358 50 314 8808.

ORCID

Monica Passananti: 0000-0003-4053-1191

Nanna Myllys: 0000-0003-0384-7277

Theo Kurtén: 0000-0002-6416-4931

Present Address

§Department of Chemistry, University of California, Irvine, California 92697−2025, United States

Notes

The authors declare no competing financial interest.

■ ACKNOWLEDGMENTS

We thank the ERC Projects 692891-DAMOCLES and 638703-COALA, the Academy of Finland, and the ATMATH Project, for funding, and the CSC-IT Center for Science in Espoo, Finland, for computational resources. N.M. thanks the Jenny and Antti Wihuri foundation for financial support.

■ REFERENCES

(1) Almeida, J.; Schobesberger, S.; Kürten, A.; Ortega, I. K.; Kupiainen-Määttä, O.; Praplan, A. P.; Adamov, A.; Amorim, A.; Bianchi, F.; Breitenlechner, M.; et al. Molecular understanding of

DOI: 10.1021/acs.jpca.8b10744
J. Phys. Chem. A 2019, 123, 611−624

sulphuric acid-amine particle nucleation in the atmosphere. *Nature* **2013**, *502*, 359−363.
(2) Bianchi, F.; Tröstl, J.; Junninen, H.; Frege, C.; Henne, S.; Hoyle, C. R.; Molteni, U.; Herrmann, E.; Adamov, A.; Bukowiecki, N.; et al. New particle formation in the free troposphere: A question of chemistry and timing. *Science* **2016**, *352*, 1109.
(3) Ehn, M.; Thornton, J. A.; Kleist, E.; Sipilä, M.; Junninen, H.; Pullinen, I.; Springer, M.; Rubach, F.; Tillmann, R.; Lee, B.; et al. A large source of low-volatility secondary organic aerosol. *Nature* **2014**, *506*, 476−479.
(4) Jokinen, T.; Sipilä, M.; Junninen, H.; Ehn, M.; Lönn, G.; Hakala, J.; Petäjä, T.; Mauldin, R. L.; Kulmala, M.; Worsnop, D. R. Atmospheric sulphuric acid and neutral cluster measurements using CI-APi-TOF. *Atmos. Chem. Phys.* **2012**, *12*, 4117−4125.
(5) Junninen, H.; Ehn, M.; Petäjä, T.; Luosujärvi, L.; Kotiaho, T.; Kostiainen, R.; Rohner, U.; Gonin, M.; Fuhrer, K.; Kulmala, M.; et al. A high-resolution mass spectrometer to measure atmospheric ion composition. *Atmos. Meas. Tech.* **2010**, *3*, 1039−1053.
(6) Mcgrath, M. J.; Olenius, T.; Ortega, I.; Loukonen, V.; Paasonen, P.; Kurtén, T.; Kulmala, M.; Vehkamäki, H. Atmospheric Cluster Dynamics Code: a flexible method for solution of the birth-death equations. *Atmos. Chem. Phys.* **2012**, *12*, 2345−2355.
(7) Olenius, T.; Schobesberger, S.; Kupiainen-Määttä, O.; Franchin, A.; Junninen, H.; Ortega, I. K.; Kurtén, T.; Loukonen, V.; Worsnop, D. R.; Kulmala, M.; et al. Comparing simulated and experimental molecular cluster distributions. *Faraday Discuss.* **2013**, *165*, 75−89.
(8) Sleno, L.; Volmer, D. A. Ion activation methods for tandem mass spectrometry. *J. Mass Spectrom.* **2004**, *39*, 1091−1112.
(9) Napari, I.; Vehkamäki, H. Postcollision relaxation of small atomic clusters. *J. Chem. Phys.* **2006**, *124*, 024303.
(10) Landau, L. D.; Lifshits, E. M. *Statistical Physics, part 1*; Pergamon: Oxford, U.K., 1969.
(11) Rice, O. K.; Ramsperger, H. C. Theories of unimolecular gas reactions at low pressures. *J. Am. Chem. Soc.* **1927**, *49*, 1617−1629.
(12) Rice, O. K.; Ramsperger, H. C. Theories of unimolecular gas reactions at low pressures. II. *J. Am. Chem. Soc.* **1928**, *50*, 617−620.
(13) Kassel, L. S. Studies in homogeneous gas reactions. I. *J. Phys. Chem.* **1927**, *32*, 225−242.
(14) Marcus, R. A.; Rice, O. The kinetics of the recombination of methyl radicals and iodine atoms. *J. Phys. Chem.* **1951**, *55*, 894−908.
(15) Baer, T.; Hase, W. L. *Unimolecular Reaction Dynamics: Theory and Experiments*; Oxford University Press on Demand: 1996.
(16) Light, J. C. Phase-space theory of chemical kinetics. *J. Chem. Phys.* **1964**, *40*, 3221−3229.
(17) Weisskopf, V. Statistics and nuclear reactions. *Phys. Rev.* **1937**, *52*, 295−303.
(18) Hansen, K. *Statistical Physics of Nanoparticles in the Gas Phase*; Springer Science & Business Media: 2012; Vol. *73*.
(19) Passananti, M.; Zapadinsky, E.; Kangasluoma, J.; Myllys, N.; Rissanen, M. P.; Kurtén, T.; Ehn, M.; Attoui, M.; Vehkamäki, H. How well can we predict cluster fragmentation inside an Atmospheric Pressure interface Time of Flight mass spectrometer? *Angew. Chem.* Submitted for publication.
(20) Wang, X.; Nicholas, J.; Wang, L. Photoelectron spectroscopy and theoretical calculations of SO_4^- and HSO_4^-: Confirmation of high electron affinities of SO_4 and HSO_4. *J. Phys. Chem. A* **2000**, *104*, 504−508.
(21) Kurtén, T.; Kuang, C.; Gómez, P.; McMurry, P. H.; Vehkamäki, H.; Ortega, I.; Noppel, M.; Kulmala, M. The role of cluster energy nonaccommodation in atmospheric sulfuric acid nucleation. *J. Chem. Phys.* **2010**, *132*, 024304.
(22) Chesnavich, W. J.; Bowers, M. T. Statistical phase space theory of polyatomic systems. Application to the cross section product kinetic energy distribution of the reaction $C_2H_4^{+}\cdot$ + C2H4 → $C_3H_5^{+}$ CH_3. *J. Am. Chem. Soc.* **1976**, *98*, 8301−8309.
(23) Chesnavich, W. J.; Bowers, M. T. Statistical phase space theory of polyatomic systems: Rigorous energy and angular momentum conservation in reactions involving symmetric polyatomic species. *J. Chem. Phys.* **1977**, *66*, 2306−2315.
(24) Chesnavich, W. J.; Bowers, M. T. Statistical phase space theory of polyatomic systems. Application to the unimolecular reactions $C_6H_5CN^{+}\cdot$ → $C_6H_4^{+}\cdot$ + HCN and $C_4H_6^{+}\cdot$ → $C_3H_3^{+}$ + $\cdot CH_3$. *J. Am. Chem. Soc.* **1977**, *99*, 1705−1711.
(25) Calvo, F.; Parneix, P. Statistical evaporation of rotating clusters. I. Kinetic energy released. *J. Chem. Phys.* **2003**, *119*, 256−264.
(26) Parneix, P.; Calvo, F. Statistical evaporation of rotating clusters. II. Angular momentum distribution. *J. Chem. Phys.* **2003**, *119*, 9469−9475.
(27) Calvo, F.; Parneix, P. Statistical evaporation of rotating clusters. III. Molecular clusters. *J. Chem. Phys.* **2004**, *120*, 2780−2787.
(28) Desloge, E. A. Classical partition function of a rigid rotator. *Am. J. Phys.* **1984**, *52*, 261−262.
(29) Chesnavich, W. J.; Su, T.; Bowers, M. T. Collisions in a noncentral field: a variational and trajectory investigation of ion-dipole capture. *J. Chem. Phys.* **1980**, *72*, 2641−2655.
(30) Elm, J.; Myllys, N.; Hyttinen, N.; Kurtén, T. Computational study of the clustering of a cyclohexene autoxidation product C6H8O7 with itself and sulfuric acid. *J. Phys. Chem. A* **2015**, *119*, 8414−8421.
(31) Stewart, J. J. Optimization of parameters for semiempirical methods V: modification of NDDO approximations and application to 70 elements. *J. Mol. Model.* **2007**, *13*, 1173−1213.
(32) Perdew, J. P.; Wang, Y. Accurate and simple analytic representation of the electron-gas correlation energy. *Phys. Rev. B: Condens. Matter Mater. Phys.* **1992**, *45*, 13244.
(33) Frisch, M. J. et al. *Gaussian16*, Revision A.03; 2016.
(34) Myllys, N.; Elm, J.; Halonen, R.; Kurtén, T.; Vehkamaki, H. Coupled cluster evaluation of the stability of atmospheric acid-base clusters with up to 10 molecules. *J. Phys. Chem. A* **2016**, *120*, 621−630.
(35) Riplinger, C.; Pinski, P.; Becker, U.; Valeev, E. F.; Neese, F. Sparse maps−A systematic infrastructure for reduced-scaling electronic structure methods. II. Linear scaling domain based pair natural orbital coupled cluster theory. *J. Chem. Phys.* **2016**, *144*, 024109.
(36) Neese, F. The ORCA program system. *Wiley Interdiscip. Rev. Comput. Mol. Sci.* **2012**, *2*, 73−78.
(37) Beyer, T.; Swinehart, D. Algorithm 448: number of multiply-restricted partitions. *Commun. ACM* **1973**, *16*, 379−379.
(38) Green, N. *Comprehensive Chemical Kinetics: Unimolecular Kinetics, Part 1. The Reaction Step*; Elsevier: 2003; Vol. *39*.
(39) Lide, D. R., Ed. *CRC Handbook of Chemistry and Physics*, 83rd ed.; CRC Press: Boca Raton, FL, 2002.
(40) Spelsberg, D.; Meyer, W. Static dipole polarizabilities of N2, O2, F2, and H2O. *J. Chem. Phys.* **1994**, *101*, 1282−1288.
(41) Vetier, A. Probability Theory with Simulations. http://math.bme.hu/~vetier/df/.

DOI: 10.1021/acs.jpca.8b10744
J. Phys. Chem. A 2019, 123, 611−624